

Equatorial symmetry breaking and the loss of dipolarity in rapidly rotating dynamos

Ferran Garcia , Ludivine Oruba & Emmanuel Dormy

To cite this article: Ferran Garcia , Ludivine Oruba & Emmanuel Dormy (2017) Equatorial symmetry breaking and the loss of dipolarity in rapidly rotating dynamos, *Geophysical & Astrophysical Fluid Dynamics*, 111:5, 380-393, DOI: [10.1080/03091929.2017.1347785](https://doi.org/10.1080/03091929.2017.1347785)

To link to this article: <http://dx.doi.org/10.1080/03091929.2017.1347785>



Published online: 10 Jul 2017.



Submit your article to this journal [↗](#)



Article views: 15



View related articles [↗](#)



View Crossmark data [↗](#)



Equatorial symmetry breaking and the loss of dipolarity in rapidly rotating dynamos

Ferran Garcia^a , Ludivine Oruba^b , Emmanuel Dormy^c 

^aDepartament de Física, Universitat Politècnica de Catalunya, Barcelona, Spain; ^bDépartement de Physique, École Normale Supérieure, Paris, France; ^cDépartement de Mathématiques et Applications, UMR-8553, École Normale Supérieure, Paris, France

ABSTRACT

Numerical studies of convection driven dynamos in rotating spherical shells exhibit a transition from steady dipolar to reversing multipolar dynamos as the forcing is increased. The dipolar-multipolar transition has so far been characterized using purely hydrodynamic parameters (Christensen and Aubert, *Geophys. J. Int.* 2006, **166**, 97–114, Soderlund *et al.*, *Earth Planet. Sci. Lett.* 2012, **333–334**, 9–20, Oruba and Dormy, *Geophys. Res. Lett.* 2014, **41**, 7115–7120). Motivated by these earlier descriptions, we investigate the hydrodynamic transitions occurring at the critical parameters. We show that the loss of dipolarity in dynamos is associated with a purely hydrodynamic transition, characterized by a breaking of the flow equatorial symmetry. Contrary to earlier expectations, we show by varying the Prandtl number that the transition is not necessarily associated with a degradation of the flow helicity.

ARTICLE HISTORY

Received 25 January 2017
Accepted 24 June 2017

KEYWORDS

Thermal convection;
convection driven dynamos;
rotating spherical shells;
dipolar-multipolar
transition; symmetry
breaking

1. Introduction

Numerical models for the Geodynamo are usually performed in the context of thermal convection in a rapidly rotating shell. Numerous studies have been undertaken, both in purely hydrodynamic and magnetohydrodynamic configurations (see Christensen 2010, Jones 2011, Nataf and Schaeffer 2015, for reviews). Kutzner and Christensen (2002) first pointed out the existence of a transition in such numerical dynamo models, between a dipolar and a multipolar regime. At low forcing, they observed a regime characterized by a large-scale steady dipolar magnetic field, superseded, for more vigorous forcing, by a small-scale multipolar field exhibiting chaotic reversals of the dipolar component. The existence of this transition has been argued to be a possible reason for reversals of the Earth's magnetic field (Christensen 2010). Further numerical studies revealed that the transition occurs sharply at a given local Rossby number, measuring the relative strengths of Coriolis and inertial forces. This has been reported with no-slip (Christensen and Aubert 2006) as well as stress-free boundary conditions (Schrinner *et al.* 2012). Schrinner *et al.* (2012) also demonstrated that the same transition could be achieved varying the aspect ratio at fixed forcing. Recently, Soderlund *et al.* (2012) pointed out that the transition

was also related to the relative strength of inertial to viscous forces. These two apparently contradictory results were reconciled in [Oruba and Dormy \(2014b\)](#) by means of a three terms balance between the non-gradient parts of the Coriolis, viscous and inertial forces at the transition.

Following the idea that the dipole collapse is well described by purely hydrodynamic parameters, the appearance of the multipolar regime was associated in [Soderlund *et al.* \(2012\)](#) (see also [Soderlund *et al.* 2014](#)) to the degradation of the flow helicity. Their work shows, in a study covering two orders of magnitude in Ekman number E , both the magnetic Prandtl number Pm and the Prandtl number Pr being fixed ($Pm = 5$ and $Pr = 1$), that dipolar fields regimes exhibit a strong relative helicity when compared to multipolar solutions. This observation should be related to the study of [Sreenivasan and Jones \(2011\)](#) which indicate that a dipolar magnetic field can act to enhance the helicity of the flow.

In this article, we compare magnetohydrodynamic dynamos and purely hydrodynamic simulations. We argue that the loss of dipolarity is associated with a purely hydrodynamic transition: the breaking of the flow equatorial symmetry. By varying the Prandtl number, we also show that the transition is not necessarily related to a degradation of the flow helicity.

2. The dynamo and hydrodynamic models

We consider a spherical electrically conducting fluid shell thermally driven by an imposed difference of temperature between the inner and outer spheres, rotating about an axis of symmetry with constant angular velocity $\boldsymbol{\Omega} = \Omega \mathbf{e}_z$, and subject to a radial gravity profile $\mathbf{g} = -g_0 r/r_0 \mathbf{e}_r$. Numerical models used in this study correspond either to purely hydrodynamic thermal convection simulations (hydrodynamic models), or to self-exciting dynamo simulations (dynamo models). The latter correspond to a wide database gathering simulations kindly provided by U. Christensen and additional simulations published in [Schinnerer *et al.* \(2012\)](#). The governing equations for the velocity, \mathbf{v} , the temperature, T , and magnetic field, \mathbf{B} , can be written in their non-dimensional form by using the gap width $L = r_o - r_i$ as unit of length, the difference of temperature ΔT between the inner and outer boundaries as unit of temperature, L^2/κ as unit of time, and $(\kappa\Omega\rho\mu)^{1/2}$ as unit for the magnetic field, κ being the thermal diffusivity, ρ the density of the fluid, μ the magnetic permeability and r_i and r_o the inner and outer radii, respectively. In the rotating reference frame and under the Boussinesq approximation, this yields

$$\frac{E}{Pr} [\partial_t \mathbf{v} + (\mathbf{v} \cdot \nabla) \mathbf{v}] = -\nabla \pi + E \nabla^2 \mathbf{v} - 2 \mathbf{e}_z \times \mathbf{v} + RaE T \frac{r}{r_o} \mathbf{e}_r + (\nabla \times \mathbf{B}) \times \mathbf{B}, \quad (1a)$$

$$\partial_t T + \mathbf{v} \cdot \nabla T = \nabla^2 T, \quad (1b)$$

$$\partial_t \mathbf{B} = \nabla \times (\mathbf{v} \times \mathbf{B}) + \frac{Pr}{Pm} \nabla^2 \mathbf{B}, \quad (1c)$$

$$\nabla \cdot \mathbf{v} = 0, \quad \nabla \cdot \mathbf{B} = 0. \quad (1d)$$

System (1) involves four non-dimensional parameters, the Rayleigh number $Ra = g_0 \alpha \Delta T L^3 / \nu \kappa$, the Prandtl number $Pr = \nu / \kappa$, the magnetic Prandtl number $Pm = \nu / \eta$, and the Ekman number $E = \nu / \Omega L^2$, with ν being the kinematic viscosity, η the magnetic

diffusivity, α the thermal expansion coefficient, and g_0 is the gravity at the outer bounding sphere. Mechanical boundary conditions are no-slip, and the outer domain is insulating. Most dynamo simulations are performed with an insulating inner core; a few of them involve a conducting inner core with the same conductivity as the fluid.

The hydrodynamic model corresponds to system (1) in the absence of magnetic field (see Garcia *et al.* 2014, for more details on the simulations being performed). In both numerical codes, equations are integrated using pseudo-spectral methods. They are discretized using spherical harmonics in the angular coordinates, and either a collocation method or a finite-difference approach in the radial direction. In both configurations, the aspect ratio χ ($\chi = r_i/r_o$) is set to the value of 0.35 (relevant to the Earth's outer core). The parameter range covered by the dynamo database is $\text{Pr} \in [0.1, 100]$, $\text{E} \in [10^{-6}, 10^{-3}]$ and $\text{Pm} \in [0.04, 66.7]$, and hydrodynamic models correspond to $\text{Pr} \in [0.025, 1]$ and $\text{E} \in [8.16 \times 10^{-6}, 10^{-4}]$. The typical estimates for the Earth's outer core are $\text{Pr} = 0.1$, $\text{E} = 10^{-14}$ and $\text{Pm} = 10^{-6}$. Computational limitations impose, for all existing models, severe constraints on the Ekman number and the magnetic Prandtl number. The Prandtl number can be more easily varied, but most numerical work focuses on the $\text{Pr} = 1$ case.

Here we cover a wide range of Prandtl number (between 10^{-1} and 10^2). As noted above, the relevant value of the Prandtl number for thermal convection in the Earth's core can be estimated to $\text{Pr} = \text{O}(10^{-1})$. If however compositional convection is being considered, the same equations remain relevant, but the equivalent ratio to the Prandtl number, then called the Schmidt number, can be estimated to be $\text{O}(10^2)$ (see Pozzo *et al.* 2012, 2013). There is thus a strong geophysical motivation to try and understand the effect of varying Prandtl numbers.

3. The dipolar-multipolar transition in dynamo models

The dipolar-multipolar transition occurs roughly at a fixed value of the local Rossby number, defined as $\text{Ro}_\ell = \text{Ro}/\ell$, where Ro is the usual Rossby number defined as the time average of $\text{Ro} = \langle \mathbf{v}^2 \rangle^{1/2}$ (the brackets denote the volume average over the shell), and ℓ is a typical length scale. Christensen and Aubert (2006) introduced a proxy for the typical length scale, $\ell_u = \pi/\bar{n}$, where \bar{n} is the mean spherical harmonics degree n in the time-averaged kinetic energy spectrum. More recently, Oruba and Dormy (2014a) used the time-averaged length scale

$$\ell_u^2 = \frac{\langle \mathbf{v}^2 \rangle}{\langle (\nabla \times \mathbf{v})^2 \rangle}. \quad (2)$$

The length scales $\tilde{\ell}_u$ and ℓ_u allow to define the local Rossby numbers $\text{Ro}_{\tilde{\ell}_u}$ and Ro_{ℓ_u} , respectively. The third quantity that will be considered in the following is $\text{RoE}^{-1/3}$, as introduced in Oruba and Dormy (2014b), which traduces the three-terms balance between the non-gradient part of the Coriolis, viscous and inertial forces at the transition. This last parameter has the advantage of not involving any a posteriori measured length scale. The dipolarity of the magnetic field f_{dip} , defined as the time-averaged ratio of the mean dipole field strength to the field strength in harmonic degrees $l = 1 - 12$ at the outer boundary (see Christensen and Aubert 2006), is represented in figure 1(a)–(c) for these three parameters. Oruba and Dormy (2014b) presented very similar figures, but restricted to the case $\text{Pr} = 1$. As already pointed out in Christensen and Aubert (2006) and Oruba and Dormy (2014b), the loss of dipolarity ($f_{\text{dip}} < 0.5$) roughly corresponds to $\text{Ro}_{\tilde{\ell}_u} \simeq 0.1$,

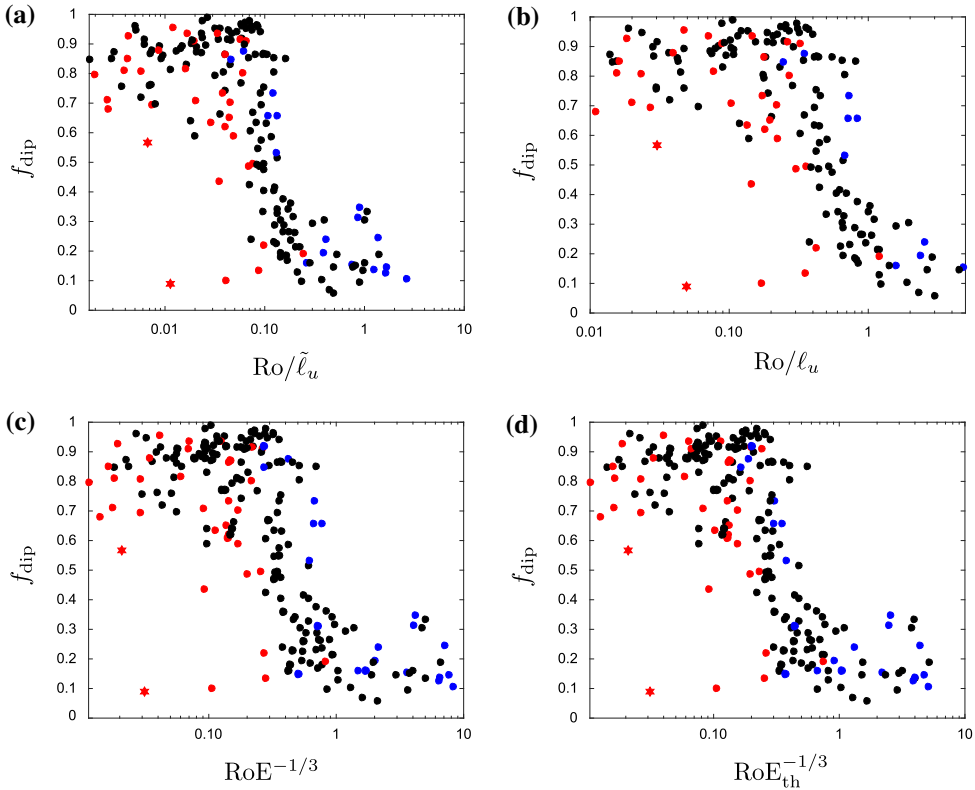


Figure 1. Dipolarity as a function of (a) the local Rossby number $Ro_{\tilde{\ell}_u}$ as defined in Christensen and Aubert (2006), (b) the local Rossby number Ro_{ℓ_u} as defined in Oruba and Dormy (2014b), (c) the parameter $RoE^{-1/3}$ (same reference) and (d) the parameter $RoE_{th}^{-1/3}$. (Colour online)

Notes: Black points correspond to $Pr = 1$, blue points to $Pr < 1$ and red points to $Pr > 1$. The stars highlight the larger value for the Prandtl number: $Pr = 100$.

$Ro_{\ell_u} \simeq 1$ and $RoE^{-1/3} \simeq 1$. The dependence on the Prandtl number is here highlighted with a colour code.

Figure 1(a) corresponds to a direct estimate, from the numerics, of the convective length scale. Figure 1(b) is a little bit more general in that it only involves a ratio of energy to enstrophy to estimate the length scale. Figure 1(c) is even more general, in that it does not involve any measured length scale, but an a priori estimate of the convective length scale based on the Ekman number. It should be noted that the dispersion with the Prandtl number appears to widen as one move from measured length scale (figure 1(a)) to estimated length scale (figure 1(c)). For this reason, we will introduce a fourth estimate of the length scale, which does not only involve the viscous length scale $E^{1/3}$, but also takes into account the thermal driving. A refined estimate is difficult for such intricate situation, so we will simply introduce a thermal convection length scale relying here on the estimate for the azimuthal length scale at the onset of convection as derived by Busse (1970) (see also Zhang 1992)

$$\ell_{th} \sim \left(E \frac{(1 + Pr)}{Pr} \right)^{1/3} \equiv E_{th}^{1/3}. \quad (3)$$

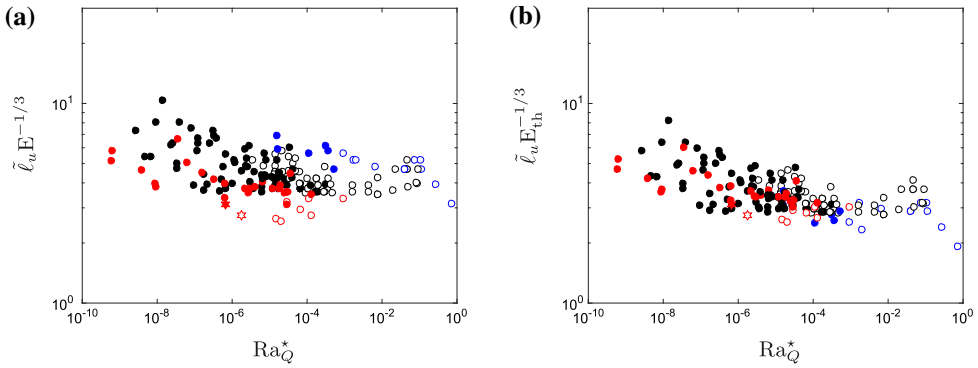


Figure 2. Scaled characteristic length scales (a) $\tilde{\ell}_u E^{-1/3}$ and (b) $\tilde{\ell}_u E_{th}^{-1/3}$, vs. the flux-based Rayleigh number, Ra_Q^* . (Colour online)

Notes: Black points correspond to $Pr = 1$, blue points to $Pr < 1$ and red points to $Pr > 1$. The stars highlight the extreme value $Pr = 100$. Full (resp. open) symbols denote dipolar (resp. multipolar) dynamos.

Figure 1(d) presents the transition, once this correction is included, and the outcome is of similar quality as figure 1(a). This suggests that when the Prandtl number is varied away from unity, ℓ_{th} offers a better a priori description of the typical length scale of the convective flow (even away from the onset of convection) than $E^{1/3}$. This can be further validated by considering figure 2, which presents the convective length scale of the flow as measured in the numerics with $\tilde{\ell}_u$ rescaled with $E^{1/3}$ and $E_{th}^{1/3}$ respectively, as a function of the so-called flux-based Rayleigh number, denoted as Ra_Q^* (introduced in Christensen and Aubert 2006). While a dispersion exists on both graphs, probably due to magnetic effects, the length scale ordering with the Prandtl number is severely reduced when $E_{th}^{-1/3}$ is used.

4. The equatorial symmetry breaking in hydrodynamic models

As shown in the previous section, the change between a dipolar and multipolar topology of the magnetic field is controlled by purely hydrodynamic parameters, namely $Ro_{\tilde{\ell}_u}$, Ro_{ℓ_u} , $RoE^{-1/3}$ and $RoE_{th}^{-1/3}$. This transition was never reported to depend on magnetic parameters (magnetic Prandtl number, Elsasser number, ...). This fact is consistent with the observation that the Lorentz force appears to have a relatively small importance on the flow in this parameters regime (Soderlund *et al.* 2012). This motivates this study which is based in a direct comparison with purely hydrodynamic simulations.

A natural question to ask is then whether a purely hydrodynamic transition occurs in the flow at similar values of $Ro_{\tilde{\ell}_u}$, Ro_{ℓ_u} , $RoE^{-1/3}$ and $RoE_{th}^{-1/3}$ as those for which the loss of dipolarity is observed in dynamo solutions?

Except at very low Prandtl numbers (Garcia *et al.* 2008), thermal convection near the onset is known to be symmetric with respect to the equator (Busse 1970, Jones *et al.* 2000, Dormy *et al.* 2004). This symmetry will eventually be broken as the Rayleigh number is increased toward sufficiently large values. This prompted us to investigate the equatorial symmetry in our simulations. We therefore introduce the time and volume averaged kinetic energy density contained in the symmetric part of the flow, denoted as K_s , which will be compared with the total kinetic energy density, K . Figure 3 shows the variation of this ratio vs. the parameters controlling the dipolar-multipolar transition, introduced in section 3.

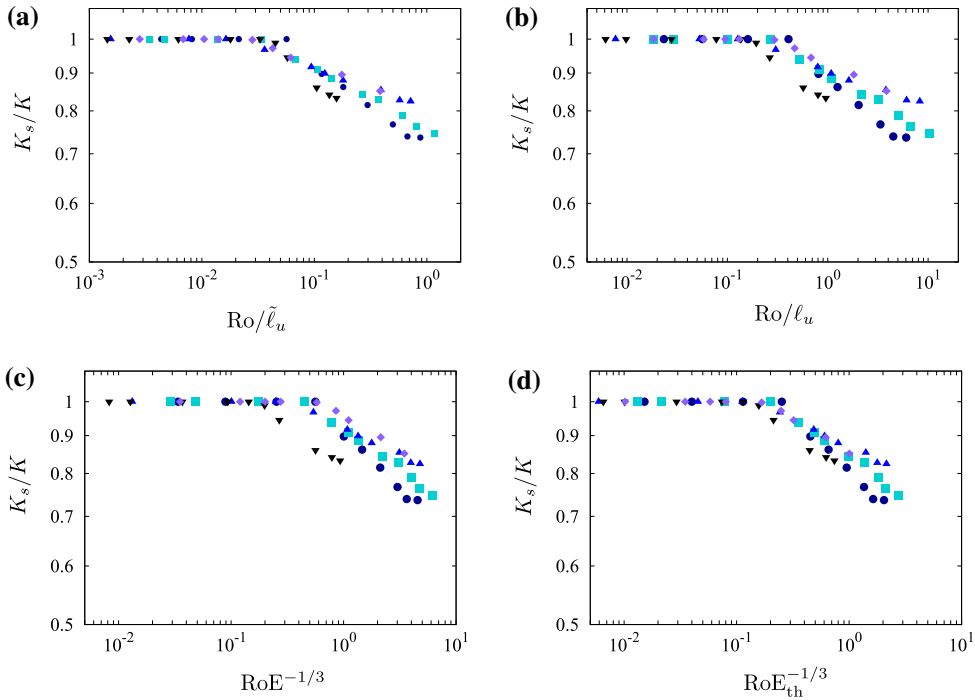


Figure 3. Ratio of the mean kinetic energy contained in the equatorially symmetric modes over the total mean kinetic energy, vs. (a) the local Rossby number Ro/ℓ_u , (b) the local Rossby number Ro/ℓ_u' , (c) the parameter $RoE^{-1/3}$ and (d) the parameter $RoE_{th}^{-1/3}$. (Colour online)

Notes: Black points correspond to $Pr = 1$, blue points to $Pr < 1$. The symbols mean \bullet $Pr = 0.1, E = 10^{-4}$; \blacksquare $Pr = 0.1, E = 3.16 \times 10^{-5}$; \blacktriangle $Pr = 0.1, E = 8.16 \times 10^{-6}$; \blacklozenge $Pr = 0.025, E = 10^{-5}$; and \blacktriangledown , $Pr = 1, E = 3.16 \times 10^{-5}$.

A breaking of the equatorial symmetry ($K_s/K < 1$) clearly occurs beyond a critical value. As in figure 1, panel 3(d) offers a similar description of the loss of symmetry as panel 3(a), without involving measured length scales. The comparison with figure 1 also shows that for each set of parameters, the threshold value is comparable to that of the dipolar-multipolar transition. In addition, the Pr dependence of critical values at the transition is indeed similar for both transitions.

In order to further characterize the breaking of the equatorial symmetry in purely hydrodynamic models, we investigate the forces balances at work, in terms of their non-gradient part. The time-averaged and volume-averaged non-gradient part of the Coriolis, $\nabla \times \mathcal{F}_c$, viscous, $\nabla \times \mathcal{F}_v$, and inertial, $\nabla \times \mathcal{F}_I$ forces are represented in figure 4, as a function of Ra/Ra_c , for the five sets of parameters $[Pr, E]$ of the hydrodynamic database. A vertical line indicates the loss of the equatorial symmetry, defined by the criterium $K_s/K < 0.9$. For all sets of parameters, the symmetric flow is characterized by a dominant balance between the non-gradient part of the Coriolis and viscous forces, as is the case in the dipolar dynamo regime. The non-gradient part of inertial forces $\nabla \times \mathcal{F}_I$ progressively increases until reaching a three terms balance at values of Ra/Ra_c slightly smaller than the threshold value corresponding to the loss of equatorial symmetry (denoted by the solid vertical line). Beyond this value, the three terms balance no longer holds, the inertial forces becoming dominant, as in the multipolar dynamo regime (see also figure 5). The change

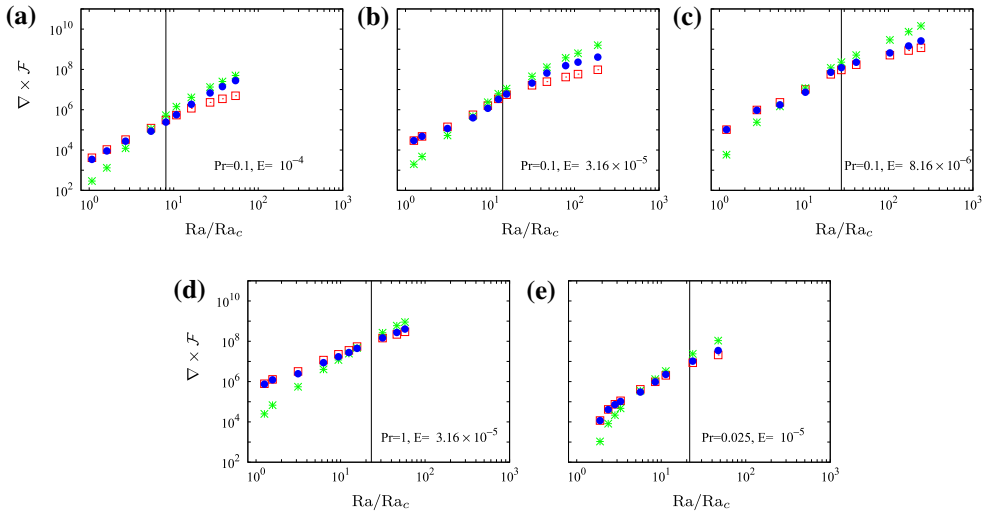


Figure 4. (a) RMS curl of forces integrals $\nabla \times \mathcal{F}_I$ (*, Inertial), $\nabla \times \mathcal{F}_C$ (\square , Coriolis) and $\nabla \times \mathcal{F}_V$ (\bullet , viscous) in purely hydrodynamic simulations, for (a) [Pr = 0.1, E = 10^{-4}], (b) [Pr = 0.1, E = 3.16×10^{-5}], (c) [Pr = 0.1, E = 8.16×10^{-6}], (d) [Pr = 1, E = 3.16×10^{-5}] and (e) [Pr = 0.025, E = 10^{-5}]. (Colour online)

Notes: The vertical line indicates the critical value for the loss of the equatorial symmetry (see figure 3).

in curl of forces balance occurs for $K_s/K < 0.9$. It thus seems that small deviations (of less than 10%) in the symmetry of the flow can occur before the change in the dominant forces occurs.

To further highlight the role of inertia after the breaking of the equatorial symmetry, we compare in figure 5 both regimes of their typical length scale $\tilde{\ell}_u$ rescaled with $E^{1/3}$, and with $E_{th}^{1/3}$, plotted as a function of the flux-based Rayleigh number.

In the symmetric regime, as expected, both quantities are roughly constant. Figure 5(b) clearly shows that $E_{th}^{1/3}$ offers a much better a priori description of the convection length scale than $E^{1/3}$ (figure 5(a)). As the solutions loose their equatorial symmetry, their characteristic length scale starts to decrease with increasing Ra_Q^* . The points in this regime appear to collapse on a single line corresponding to a $Ra_Q^{*-1/5}$ scaling. This corresponds, as identified by Garcia *et al.* (2014), to the inertial scaling $Ro \sim Ra_Q^{*2/5}$, derived from the IAC balance (Aubert *et al.* 2001, Jones 2011). The $Ra_Q^{*-1/5}$ scaling thus reflects the $Ro^{-1/2}$ scaling, stemming from the balance between the non-gradient part of Coriolis and inertial forces beyond the transition.

It is interesting to establish a deeper comparison of both transitions in terms of their dependence on the Prandtl number. For this purpose, for each data set corresponding to a given value of Pr, we compute the critical values of $Ro_{\tilde{\ell}_u}$, Ro_{ℓ_u} , $RoE^{-1/3}$ and $RoE_{th}^{-1/3}$ at which the transitions occur. This results in figure 6, where black (resp. red) points denote the dynamo-multipolar (resp. hydrodynamic) transition.

The first important thing to be noticed is that, as pointed in the previous section, both transitions occur at similar values of the control parameters (see for example the Pr = 0.1 and Pr = 1 cases in figure 6, for which both dynamo and hydrodynamic data are available). The transition values on all four graphs are not expected to vary significantly between the hydrodynamic simulations and the dynamo simulations, as it is now well established that

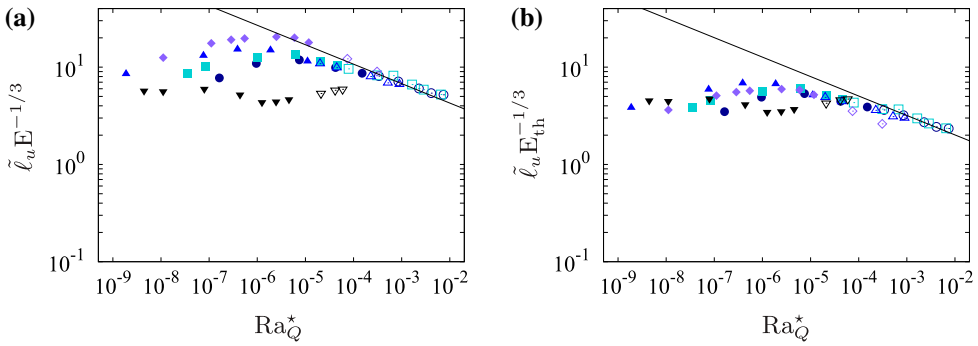


Figure 5. Scaled characteristic length scales (a) $\tilde{\ell}_u E^{-1/3}$ and (b) $\tilde{\ell}_u E_{th}^{-1/3}$, vs. the flux-based Rayleigh number, Ra_Q^* . (Colour online)

Notes: Black points correspond to $Pr = 1$, blue points to $Pr < 1$. Full (resp. open) symbols denote symmetric (resp. non-symmetric) flows. The solid line represents the $Ra_Q^*{}^{-1/5}$ scaling. Same symbols as in figure 2.

in these models, the typical length-scale of convection is not significantly altered by the presence of the magnetic field. Also note that in a similar way as in figures 1 and 3, figure 6(d) offers a description of the transition comparable to that of figure 6(a), without involving measured length scales. The second important point is that both transitions exhibit the same dependence on Pr . As identified in section 3, the critical values of $Ro_{\tilde{\ell}_u}$, Ro_{ℓ_u} , $RoE^{-1/3}$ and $RoE_{th}^{-1/3}$ monotonically decrease with increasing Pr . The behaviour however depends on whether Pr is less than unity, or not. For $Pr < 1$, it is almost flat; in the low Prandtl number limit, the critical values thus roughly correspond to the values at $Pr = 1$, i.e. $Ro_{\tilde{\ell}_u} \simeq 0.1$, $Ro_{\ell_u} \simeq 1$, $RoE^{-1/3} \simeq 1$ and $RoE_{th}^{-1/3} \simeq 1$. This is not the case at larger Prandtl numbers, for which the critical values decay significantly as Pr increases. The fact that the critical value for transition still exhibits a Pr dependence on all four panels probably indicates that more than one length scale is present in the convective flow, for example a radial and an azimuthal length scale (e.g. Zhang 1992), and that the ratio between these length scales may vary with the Prandtl number. We only rely here on an estimate, based on the azimuthal length scale at the onset, and which appears to provide an adequate description of the flow.

5. Dynamo mechanisms

It is interesting to understand how changes in the flow are related to changes in dynamo action. A useful tool to analyse the dynamo mechanisms is to use mean-field formalism. This has been investigated in Schinnerer *et al.* (2012). They have shown that the loss of dipolarity was related to a sudden collapse of the γ -effect, and not to an alteration of the α -effect. A proxy often used to measure the α -effect is the kinetic helicity. Schinnerer *et al.* (2007) however showed that the kinetic helicity does not provide a good approximation in the case of geodynamo models. The link between the α -effect and helicity requires either that the magnetic diffusion time is long compared to the induction time, or that the turnover time is long compared to the correlation time (e.g. Moffatt 1978; Moffatt 2014). Whereas Schinnerer *et al.* (2012) do not report a collapse of the α -effect, Soderlund *et al.* (2012) noted a significant degradation of the relative kinetic helicity at the transition to

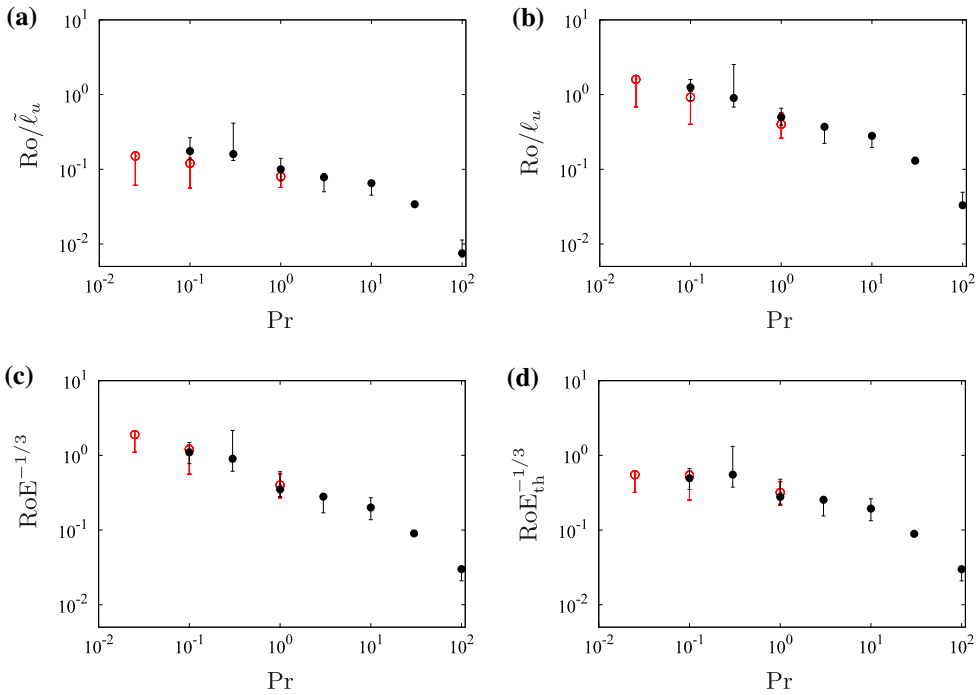


Figure 6. Pr dependence of the dipolar-multipolar transition in dynamo simulations (in black), and of the loss of equatorial symmetry in hydrodynamic simulations (in red). It shows the value of (a) the local Rossby number $Ro_{\tilde{\ell}_u}$, (b) the local Rossby number Ro_{ℓ_u} , (c) the parameter $RoE^{-1/3}$ and (d) the parameter $RoE_{th}^{-1/3}$ at the transition, as a function of Pr. (Colour online)

Notes: The black error bars indicate the ranges from the last dipolar point ($f_{dip} > 0.5$) to the first multipolar one ($f_{dip} < 0.5$), and the others those from the last symmetric point ($K_s/K > 0.9$) to the first non-symmetric one ($K_s/K < 0.9$). The dots stem from a linear interpolation.

multipolar dynamos. Besides, numerical studies have stressed that the presence of a mean helicity in a numerical model is not necessarily related to that of a large-scale dipolar field (Livermore *et al.* 2007).

In order to further clarify the helicity behavior at the transition, we investigate hydrodynamic simulations performed at $Pr = 1$ and at lower Prandtl numbers, $Pr = 0.1$ and $Pr = 0.025$. Following Soderlund *et al.* (2012), we consider the instantaneous axial helicity

$$H_z = v_z \omega_z, \tag{4}$$

and compute its volumetric average over the mainstream flow, i.e. excluding the boundary layers, denoted as $\langle \cdot \rangle^*$ in following. As $\langle H_z \rangle^*$ vanishes in the case of symmetric flows, we consider the quantity $|H_z|$, defined as

$$|H_z| = \frac{1}{2} \left(\langle H_z \rangle_{NH}^* - \langle H_z \rangle_{SH}^* \right), \tag{5}$$

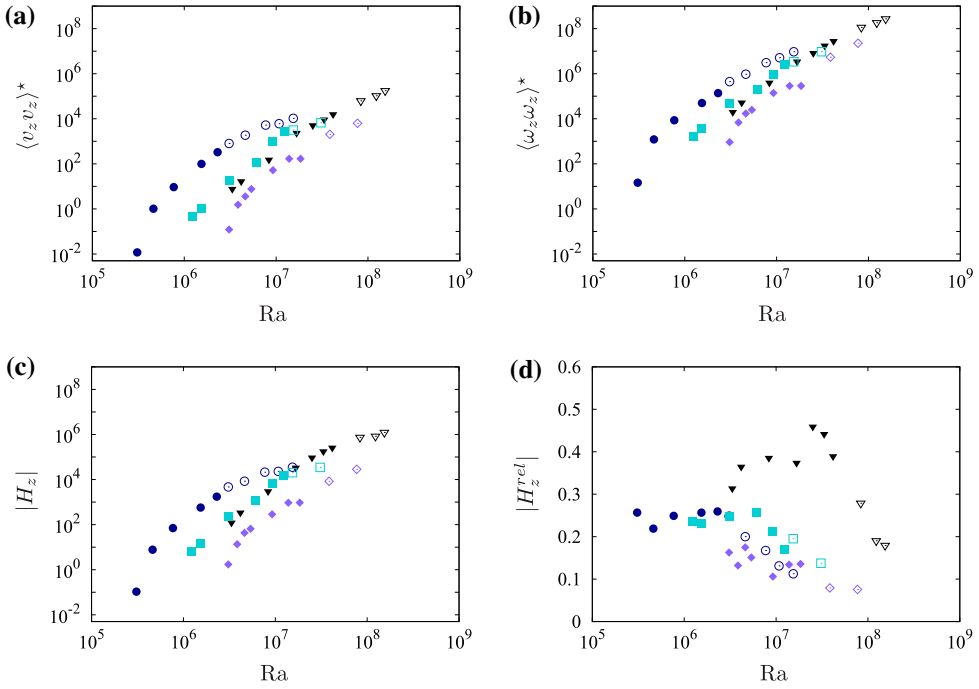


Figure 7. Instantaneous quantities (a) $\langle v_z v_z \rangle^*$, where v_z is the axial velocity, (b) $\langle \omega_z \omega_z \rangle^*$, ω_z being the axial vorticity, (c) the axial helicity $|H_z|$, and (d) the relative helicity $|H_z^{rel}|$, vs. the Rayleigh number Ra . (Colour online)

Notes: Black points correspond to $Pr = 1$, blue points to $Pr < 1$. Full (resp. open) symbols denote symmetric (resp. non-symmetric) flows. Same symbols as in figure 2.

where the subscripts NH (resp. HS) denote the average over the northern (resp. southern) hemispheres. We also consider the relative axial helicity defined as

$$|H_z^{rel}| = \frac{|H_z|}{(\langle v_z v_z \rangle^* \langle \omega_z \omega_z \rangle^*)^{1/2}}, \quad (6)$$

where the axial helicity has been normalized by its maximum possible value. Figure 7 shows the instantaneous quantities $\langle v_z v_z \rangle^*$, $\langle \omega_z \omega_z \rangle^*$, $|H_z|$ and $|H_z^{rel}|$, as a function of the Rayleigh number Ra . The three former quantities exhibit a monotonic increase, as Ra increases. The relative axial helicity $|H_z^{rel}|$ however exhibits a very different behaviour (see figure 7(d)). In the case $Pr = 1$, $|H_z^{rel}|$ sharply decreases very close to the transition, this behaviour was first observed and reported in Soderlund *et al.* (2012) (see also their corrigendum Soderlund *et al.* 2014). This behaviour is however not reproduced when $Pr = 0.1$, and the degradation of $|H_z^{rel}|$ is nearly absent at $Pr = 0.025$.

When $Pr = 0.1$, $|H_z^{rel}|$ is less than 30% in the symmetric regime. This fraction is even lower for $Pr = 0.025$. These flows however do maintain an equatorial symmetry and sustain a dipolar field. This corroborates the point of Schinnerer *et al.* (2007) that helicity is not a proxy for the α -effect in these configurations.

At $Pr = 1$, as pointed out by Soderlund *et al.* (2012), the transition is associated with a degradation of relative helicity in the flow. However, this picture does not hold in the low

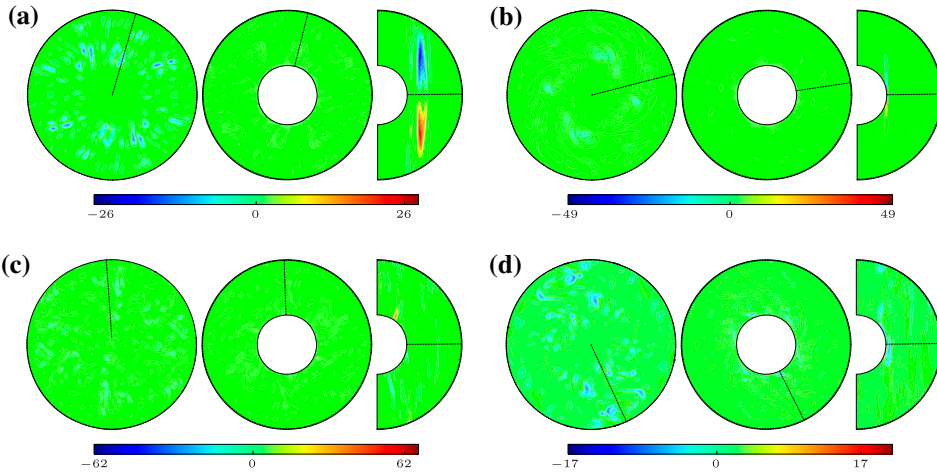


Figure 8. Contour plots of the instantaneous local relative axial helicity $H_z/(\langle v_z v_z \rangle^* \langle \omega_z \omega_z \rangle^*)^{1/2}$, corresponding to hydrodynamical solutions obtained for $E = 3.16 \times 10^{-5}$ and for four different sets of parameters $[\text{Pr}, \text{Ra}]$. Each panel shows, from left to right, spherical (at radius r_o , viewed from the north pole), equatorial and meridional sections (this last projection is made at the azimuthal angle where axial helicity is maximum; it is indicated by the dashed lines in the other projections). Panels (a) and (b) correspond to equatorially symmetric solutions obtained for $[1, 2.51 \times 10^7]$ and $[0.1, 6.15 \times 10^6]$, respectively. Panels (c) and (d) show asymmetric solutions corresponding to $[1, 8.35 \times 10^7]$ and $[0.1, 1.23 \times 10^7]$. (Colour online)

Notes: The gray scale is the same for all the contour plots corresponding to each solution, with white (red) meaning positive axial helicity.

Prandtl number regime. Besides, if by helicity we denote the axial helicity, instead of the relative axial helicity, this quantity keeps increasing beyond the transition.

Figure 8 complements figure 7, by showing the local relative axial helicity $H_z/(\langle v_z v_z \rangle^* \langle \omega_z \omega_z \rangle^*)^{1/2}$ of the hydrodynamical solutions obtained for two different values of Pr , i.e. $\text{Pr} = 1$ and $\text{Pr} = 0.1$, the Ekman number being fixed ($E = 3.16 \times 10^{-5}$). Depending on Ra , equatorially symmetric (figure 8(a),(b)), or asymmetric (figure 8(c),(d)) solutions are obtained. Figure 8(a),(c) corresponds to $\text{Pr} = 1$. At moderate forcing (figure 8(a)), the pattern of the relative axial helicity is roughly anti-symmetric across the equator. It exhibits large-scale vortices elongated in the axial direction, mainly developed within a relatively wide annulus, coaxial with the axis of rotation and tangential to the inner sphere (see the meridional section). As the forcing is increased (figure 8(c)), the equatorial symmetry is broken and the relative axial helicity is then clearly degraded. This picture is however different at $\text{Pr} = 0.1$ (figure 8(b),(d)). In that case, the relative axial helicity of the equatorially symmetric solution is nearly negligible in the bulk of the fluid. Helicity is concentrated in a small-scale structure, also elongated in the axial direction and tangent to the inner sphere (figure 8(b)). The asymmetric solution (figure 8(d)) is characterized by a weak axial helicity, as in the $\text{Pr} = 1$ case.

As noted by Christensen *et al.* (1999), the breaking of symmetry in both cases (figure 8(c),(d)) appears concomitant of the onset of convection inside the tangent cylinder. In their study, they noticed that with a strong magnetic field (in terms of Elsasser number), the Lorentz force appeared to help the onset of convection inside the cylinder tangent to the inner core.

6. Discussion and conclusions

We investigated the transition from steady dipolar to reversing multipolar dynamos observed in numerical simulations in several earlier studies. Motivated by the previous descriptions of this transition in terms of hydrodynamic quantities (Christensen and Aubert 2006), we compared full dynamo simulations to purely hydrodynamic simulations in a rotating spherical shell.

Such an approach, which suggests that in the dynamo models considered here, the Lorentz force saturates the dynamo but is not responsible for the key transitions in the flow, is supported by earlier studies (e.g. Soderlund *et al.* 2012).

The main result of our paper is that the loss of dipolarity in dynamo simulations is concomitant of a purely hydrodynamic transition, characterized by the breaking of the flow equatorial symmetry. Further investigations of the loss of symmetry and dipolarity in dynamos are deserved. We should stress the earlier study of Christensen *et al.* (1999) which was however limited to a boolean quantification of symmetry that does not allow a precise comparison with the loss of dipolarity. Based on our simulations, we argue that both transitions appear to correspond to the same forces balance, that is to say, the breaking of the leading order geostrophic balance by the inertial forces. They are characterized by the same critical values of the parameters controlling the transition. This relation between the transitions is observed for five hydrodynamic database sets in which the Prandtl and Ekman numbers roughly vary two orders of magnitude.

The threshold values do exhibit the same dependence with the Prandtl number Pr . In both configurations, they are independent on Pr for low Prandtl numbers ($Pr < 1$), but decrease when Pr increases to large values ($Pr > 1$). This points to a sole mechanism to describe both transitions. The remaining Pr dependence of the transition highlights the complexity of the length scales involved in convective flows (Zhang 1992, Jones *et al.* 2000, Dormy *et al.* 2004).

We have also shown that the transition is not necessarily associated with a degradation of the helicity in the flow. Indeed, beyond the transition, the axial helicity keeps increasing monotonically as the forcing increases. More importantly, the decrease of the relative axial helicity observed in Soderlund *et al.* (2012) at $Pr = 1$ does not hold in the low Prandtl number limit.

The symmetry breaking associated with inertial effects is directly related to the over-estimated role of inertia in numerical models for the geodynamo. It is because of these strong inertial effects, that the Lorentz force could be neglected in studying the transition. It has recently been pointed out (Dormy 2016) that reducing inertial effects could lead to more geophysically relevant forces balances. Indeed reducing inertial effects (by considering larger magnetic Prandtl numbers) opens the way to transitions associated with magnetic effects, such as the runaway field growth reported in Dormy (2016), see also Dormy *et al.* (in press).

The loss of equatorial symmetry in numerical models could however be important to understand geodynamo reversals. A key feature of the multipolar regime is the occurrence of chaotic reversals of the dipolar component. Our result, which relates the dipolar-multipolar transition to the breakdown of the flow equatorial symmetry, points to the connections of polarity reversals and a breakdown of the flow equatorial symmetry (see Petrelis *et al.*

2009). Further studies are deserved to understand how this symmetry is broken in an Earth-like parameter regime (i.e. with less inertial effects).

Acknowledgement

The authors wish to thank Pr. U. Christensen for kindly sharing his numerical database.

Disclosure statement

No potential conflict of interest was reported by the authors.

Funding

This work has been supported by Spanish MCYT/FEDER [grant number FIS2013-40674 and FIS2016-76525-P].

ORCID

Ferran Garcia  <http://orcid.org/0000-0003-4507-0486>

Ludivine Oruba  <http://orcid.org/0000-0003-0230-8634>

Emmanuel Dormy  <http://orcid.org/0000-0002-9683-6173>

References

- Aubert, J., Nataf, H.-C., Cardin, P. and Masson, J.-P., A systematic experimental study of rapidly rotating spherical convection in water and liquid gallium. *Phys. Earth Planet. Inter.* **2001**, **128**, 51–74.
- Busse, F.H., Thermal instabilities in rapidly rotating systems. *J. Fluid Mech.* **1970**, **44**, 441–460.
- Christensen, U., Dynamo scaling laws and applications to the planets. *Space Sci. Rev.* **2010**, **152**, 565–590.
- Christensen, U. and Aubert, J., Scaling properties of convection-driven dynamos in rotating spherical shells and application to planetary magnetic fields. *Geophys. J. Int.* **2006**, **166**, 97–114.
- Christensen, U., Olson, P. and Glatzmaier, G.A., Numerical modelling of the geodynamo: a systematic parameter study. *Geophys. J. Int.* **1999**, **138**, 393–409.
- Dormy, E., Strong field spherical dynamos. *J. Fluid. Mech.* **2016**, **789**, 500–513.
- Dormy, E., Oruba, L. and Pettdemange, L., Three branches of dynamo action. *Fluid Dyn. Res.*, in press.
- Dormy, E., Soward, A.M., Jones, C.A., Jault, D. and Cardin, P., The onset of thermal convection in rotating spherical shells. *J. Fluid Mech.* **2004**, **501**, 43–70.
- Garcia, F., Sánchez, J. and Net, M., Antisymmetric polar modes of thermal convection in rotating spherical fluid shells at high Taylor numbers. *Phys. Rev. Lett.* **2008**, **101**, 194,501-(1–4).
- Garcia, F., Sánchez, J. and Net, M., Numerical simulations of thermal convection in rotating spherical shells under laboratory conditions. *Phys. Earth Planet. Inter.* **2014**, **230**, 28–44.
- Jones, C.A., Planetary magnetic fields and fluid dynamos. *Annu. Rev. Fluid Mech.* **2011**, **43**, 583–614.
- Jones, C.A., Soward, A.M. and Mussa, A.I., The onset of thermal convection in a rapidly rotating sphere. *J. Fluid Mech.* **2000**, **405**, 157–179.
- Kutzner, C. and Christensen, U., From stable dipolar towards reversing numerical dynamos. *Phys. Earth Planet. Inter.* **2002**, **44**, 29–45.
- Livermore, P.W., Hughes, D.W. and Tobias, S.M., The role of helicity and stretching in forced kinematic dynamos in a spherical shell. *Phys. Fluids* **2007**, **19**, 057101.

- Moffatt, H.K., *Magnetic Field Generation in Electrically Conducting Fluids*, 1978. (Cambridge: Cambridge University Press).
- Moffatt, H.K., Helicity and singular structures in fluid dynamics. *PNAS* **2014**, **111**, 3663–3670.
- Nataf, H.C. and Schaeffer, N., Turbulence in the core. In *Treatise Geophysics*, ed. Olson, P. and Schubert, G. (Elsevier), 2nd ed. Vol. 8, pp. 161–181, **2015**.
- Oruba, L. and Dormy, E., Predictive scaling laws for spherical rotating dynamos. *Geophys. J. Int.* **2014a**, **198**, 828–847.
- Oruba, L. and Dormy, E., Transition between viscous dipolar and inertial multipolar dynamos. *Geophys. Res. Lett.* **2014b**, **41**, 7115–7120.
- Petrelis, F., Fauve, S., Dormy, E. and Valet, J.-P., Simple mechanism for reversals of Earth’s magnetic field. *Phys. Rev. Lett.* **2009**, **102**, 144503 (4).
- Pozzo, M., Davies, C., Gubbins, D. and Alfe, D. Thermal and electrical conductivity of iron at Earth’s core conditions. *Nature* **2012**, **485**, 355–358.
- Pozzo, M., Davies, C., Gubbins, D. and Alfe, D., Transport properties for liquid silicon-oxygen-iron mixtures at Earth’s core conditions. *Phys. Rev. B*, **2013**, **87**, 014110 (10).
- Schrinner, M., Radler, K.H., Schmitt, D., Rheinhardt, M. and Christensen, U.R., Mean-field concept and direct numerical simulations of rotating magnetoconvection and the geodynamo. *Geophys. Astrophys. Fluid Dyn.* **2007**, **101**, 81–116.
- Schrinner, M., Petitmange, L. and Dormy, E., Dipole collapse and dynamo waves in global direct numerical simulations. *Astrophys. J.* **2012**, **752**, 1–12.
- Soderlund, K.M., King, E.M. and Aurnou, J.M., The influence of magnetic fields in planetary dynamo models. *Earth Planet. Sci. Lett.* **2012**, **333–334**, 9–20.
- Soderlund, K.M., King, E.M. and Aurnou, J.M., Corrigendum to “The influence of magnetic fields in planetary dynamo models” [*Earth Planet. Sci. Lett.* **333–334**, 9–20]. *Earth Planet. Sci. Lett.* **2012**, **2014**, 121–123.
- Sreenivasan, B. and Jones, C.A., Helicity generation and subcritical behaviour in rapidly rotating dynamos. *J. Fluid Mech.* **2011**, **688**, 5–30.
- Zhang, K., Spiralling columnar convection in rapidly rotating spherical fluid shells. *J. Fluid Mech.* **1992**, **236**, 535–556.